EPJ manuscript No.
(will be inserted by the editor)

The prospects of sympathetic cooling of NH molecules with Li atoms

Alisdair O. G. Wallis, Edward J. J. Longdon, Piotr S. Żuchowski, and Jeremy M. Hutson

Department of Chemistry, Durham University, South Road, Durham, DH1 3LE, United Kingdom

February 23, 2011

Abstract. We calculate the quartet potential energy surface for Li+NH and use it to calculate elastic and spin-relaxation cross sections for collisions in magnetically trappable spin-stretched states. The potential is strongly anisotropic but spin-relaxation collisions are still suppressed by centrifugal barriers when both species are in spin-stretched states. In the ultracold regime, both the elastic and inelastic cross sections fluctuate dramatically as the potential is varied because of Feshbach resonances. The potential-dependence is considerably reduced at higher energies. The major effect of using an unconverged basis set in the scattering calculations is to shift the resonances without changing their general behaviour. We have calculated the ratio of elastic and spin-relaxation cross sections, as a function of collision energy and magnetic field, for a variety of potential energy surfaces. Most of the surfaces produce ratios that are favorable for sympathetic cooling, at temperatures below about 20 mK.

PACS. 34.50.Cx

1 Introduction

Since 1995, when the first gaseous Bose-Einstein condensates (BECs) were created [1,2], the ability to cool, trap, and control atoms at ultracold (sub-millikelvin) temperatures has increased dramatically. More recently, attention has turned to cold and ultracold molecules [3,4,5]. With their more complex energy structure, ultracold molecules open up many new possibilities in fields such as high-precision measurement [6,7], quantum computing [8], and ultracold chemistry [9]. However, this extra complexity comes at a price, with the extra structure making molecules more difficult to cool.

Atoms are usually cooled to microkelvin temperatures by laser Doppler cooling [10]. However laser cooling is much less effective for molecules than for atoms. For this reason, many other methods for cooling molecules have been developed. These can be categorized into two distinct types, direct and indirect methods [11,12]. Indirect methods involve the formation of ultracold molecules from a sample of precooled ultracold atoms, and deeply bound and absolute ground-state alkali-metal dimers have recently been formed, by magnetoassociation (Feshbach resonance tuning) followed by laser state transfer with Stimulated Raman Adiabatic Passage (STIRAP) [13,14,15,16]. Indirect methods are limited by the range of ultracold atoms available, mainly to molecules formed from alkali-metal atoms. Direct methods, such as buffer-gas cooling [17] and Stark deceleration [11], involve directly cooling a sample of warm molecules down towards ultracold temperatures. NH molecules have been buffer-gas cooled and magnetically trapped in their $X^3\Sigma^-$ state, both alone [18,19,20] and in combination with N atoms [21], and Stark-decelerated and electrostatically trapped in their metastable $a^1\Delta$ state [22]. Proposals exist to transfer the metastable $a^1\Delta$ molecules into the $X^3\Sigma^-$ ground state, either with an intense laser field [23] or by collisions with Rb atoms [24]. However, the lowest temperatures currently obtainable by direct methods are tens to hundreds of millikelvin, so that a secondary cooling stage is required to reach ultracold temperatures.

One possible secondary cooling method is sympathetic cooling, in which precooled cold molecules are placed in contact with an ultracold atomic coolant and allowed to thermalize. However, for sympathetic cooling to be effective, the rate of elastic (cooling) collisions must greatly exceed the rate of inelastic (trap-loss and heating) collisions [25]. As a rule of thumb, the ratio of elastic to inelastic cross sections must exceed 100. Molecules trapped in magnetic and electrostatic traps are held in low-field-seeking states (states in which the energy increases with increasing field). Collisional spin-relaxation processes from low-field to untrapped high-field-seeking states will therefore limit the efficiency of sympathetic cooling, and in many of the systems theoretically studied the rate of collisional trap loss will be too rapid for sympathetic cooling to work. Sympathetic cooling has yet to be demonstrated for neutral molecular systems. However it has been used to cool trapped ions [26,27], to produce overlapping Bose-Einstein condensates [28], and to cool fermionic [29] and bosonic [30] atoms to quantum degeneracy.

The first to consider the sympathetic cooling of molecules with alkali-metal atoms were Soldán and Hutson [31], who examined the interaction between rubidium atoms and NH($X^3\Sigma^-$). They found that the dispersion-bound states of RbNH that correspond to the Rb(^2S)+NH($X^3\Sigma^-$) dissociation threshold are crossed by deeper ion-pair states, which correspond to the $Rb^+(^1S)$ + $NH^-(^2\Pi)$ dissociation threshold. These ion-pair states introduce mechanisms for inelastic collisions and three-body recombination that may hamper sympathetic cooling. Lara *et al.* subsequently investigated the Rb(^2S)+OH($^2\Pi_{3/2}$) system [32,33] and also found ion-pair states that crossed the RbOH covalent states. They also carried out full quantum calculations of field-free low-energy collisions on the coupled potential energy surfaces and found fast spin relaxation collisions that would prevent sympathetic cooling for most states. More recently, detailed potential energy surfaces and field-free scattering calculations for Rb+NH and Cs+NH were performed by Tacconi *et al.* [34,35,36], who found large rotational inelasticities.

Sympathetic cooling of NH_3 and ND_3 has also been considered. Żuchowski and Hutson [37] surveyed the interaction potentials of NH_3 with alkali-metal and alkaline-earth atoms. They found that all the systems studied exhibited large anisotropies that would produce strong rotation-tunnelling inelasticity, so that sympathetic cooling is unlikely to be successful for NH_3 in low-field-seeking states. Żuchowski and Hutson [38] went on to examine the collisions of NH_3 and ND_3 with Rb, showing that there is a good prospect of sympathetic cooling of ND_3 in high-field-seeking states, even in collision with magnetically trapped atoms.

Lara *et al.* [33] identified several desirable features for sympathetic cooling of molecules that are not in their absolute ground state. First, it is desirable to use light atomic cooling partners, which produce high centrifugal barriers that can suppress inelastic loss in channels with a small kinetic energy release. Secondly, it is desirable to use molecules where the electron spin is weakly coupled to the intermolecular axis, such as molecules with Hund's case (b) coupling. Thirdly, it is desirable to use atom-molecule systems for which the interaction potentials are only weakly anisotropic. They suggested that closed-shell atoms such as the alkaline earths might make good collision partners for magnetically trapped molecules.

In 2009 Soldán, Żuchowski, and Hutson [39] followed up these suggestions: they chose the case (b) molecule NH($X^3\Sigma^-$) as a test case and investigated its interactions with both alkali-metal and alkaline-earth atoms. All the alkali-metal and the heavier alkaline-earth systems (Ca-NH and Sr-NH) were found to have strongly anisotropic interaction potentials, but Be-NH and Mg-NH were found to have weak anisotropy. All the systems have ion-pair states, but for Be and Mg the ion-pair states cross the dispersion-bound state high up on the repulsive wall, so that the ion-pair states will be energetically inaccessible in low-temperature collisions. Wallis and Hutson [40] then performed detailed quantum scattering calculations on Mg+NH($X^3\Sigma^-$) and showed that the ratio of elastic to inelastic cross sections is large enough to allow sympathetic cooling over a wide range of collision energies and magnetic fields. Sympathetic cooling of NH with Mg has a good prospect of success if the molecules can be precooled to 10 mK and good trap overlap can be achieved.

Part of the success of Mg as a coolant comes from the fact that its ground state has zero electron spin, so that only spin relaxation and not spin exchange is possible in collisions with NH. However, the lack of electron spin also prevents magnetic trapping. In addition, Mg is quite hard to laser-cool, though Mehlstäubler *et al.* [41] have been successful in achieving sub-Doppler temperatures. An alternative way to prevent spin exchange is to use an alkali-metal atom as the collision partner, while ensuring that all collisions are between atoms and molecules in spin-stretched states, with the maximum possible values of both electron and nuclear spin projection quantum numbers. The use of spin-stretched states also prevents strong interactions involving ion-pair states. It is important to know whether this approach would result in low enough inelastic collision rates, despite the much larger anisotropies in alkali-NH systems. Previous collision calculations on Rb+NH and Cs+NH [36] did not include the effects of magnetic fields and did not consider the spin-changing collisions that are important for sympathetic cooling.

In this paper we assess the prospects for sympathetic cooling of cold NH($X^3\Sigma^-$) molecules with ultracold Li(^2S) atoms. We choose Li as the collision partner because its low mass produces high centrifugal barriers that suppress spin-changing collisions at low energies. ^{7}Li has nuclear spin $I_{\rm Li} = 3/2$, and has a magnetically trappable spin-stretched state with total angular momentum $F = 2$ and $M_F = 2$. The ^{14}NH molecule has complicated hyperfine structure due to its electron spin $S = 1$ and two nuclear spins $I_{\rm N} = 1$ and $I_{\rm H} = 1/2$; its magnetically trappable spin-stretched state has $F = 5/2$ and $M_F = +5/2$. Collisions between spin-stretched Li and NH have $M_S = m_{s_{\rm Li}} + m_{s_{\rm NH}} = +3/2$ and thus occur entirely on the quartet surface of Li-NH. We confine our attention to these collisions. Collisions between states with $|M_S| \neq 3/2$ involve the doublet surface as well as the quartet surface and are likely to lead to fast spin exchange.

The structure of this paper is as follows. Section 2 describes electronic structure calculations of the quartet potential energy surface for Li(^2S)+NH($X^3\Sigma^-$). Section 3 describes quantum scattering calculations and Section 4 explores the prospects for sympathetic cooling.

2 Potential Energy Surface

We have calculated the quartet interaction potential for Li(^2S)+NH($X^3\Sigma^-$), using high-level *ab initio* electronic structure calculations. Calculations were performed using an open-shell spin-restricted version [42] of the coupled cluster method [43] with single, double, and perturbative triple excitations [RCCSD(T)]. We used the aug-cc-pVTZ basis set for N and H, and the uncontracted cc-pVTZ basis for the Li atom [44], augmented by Gaussian functions

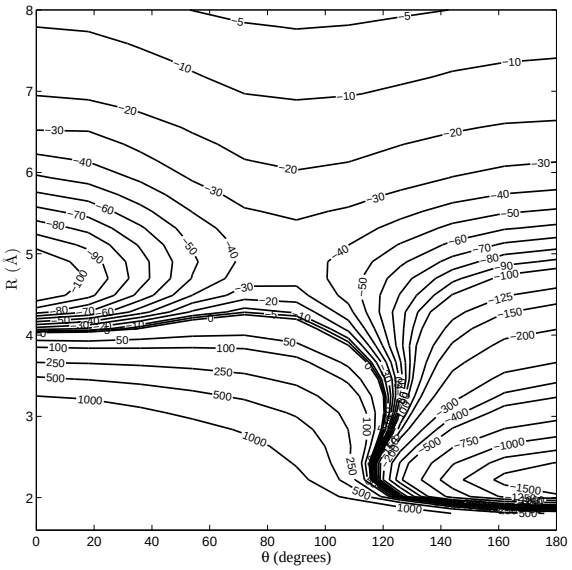

Fig. 1. Li(^2S)+NH($X^3\Sigma^-$) quartet potential energy surface. Contours are labeled in cm^{-1}. $\theta = 0°$ corresponds to the linear N-H-Li geometry.

with exponents s:0.001, p:0.008, d:0.034, and f:0.073. To improve the basis set for the Van der Waals dispersion interaction we included spd bond functions (with exponents 0.9, 0.3, 0.1 for s and p and 0.6 and 0.2 for d and f) at the Li-NH center of mass. All *ab initio* calculations were performed using the MOLPRO package [45] and corrected for basis-set superposition error using the counterpoise method of Boys and Bernardi [46].

Calculations were performed on a grid in Jacobi coordinates (R, θ), with a fixed NH bond length $r = 1.0367$ Å [47]. R is the separation between the NH center of mass and the Li atom, and θ is the angle between the NH bond vector and R, with $\theta = 0$ corresponding to the linear NH-Li geometry. The angular grid is a set of 11 angles corresponding to Gauss-Lobatto quadrature points, and the radial grid extends from high up on the repulsive potential wall to 15 Å.

For each angle, radial interpolation for $R \leq 15$ Å and extrapolation for $R > 15$ Å is performed using the reproducing kernel Hilbert space (RKHS) method [48,49] to obtain the potential for any given value of R. The potential is then expanded in Legendre polynomials,

$$V(R, \theta) = \sum_{\lambda} V_\lambda(R) P_\lambda(\cos\theta), \tag{1}$$

for $\lambda \leq 8$. The radial strength coefficients $V_\lambda(R)$ are evaluated by integrating over the angular grid at each R using Gauss-Lobatto quadrature.

Figure 1 shows the calculated quartet potential energy surface for Li-NH. The global potential minimum is about 1800 cm^{-1} deep and occurs at θ=180° (Li-NH). A secondary minimum about 113 cm^{-1} deep occurs at θ=0°. The large anisotropy is due to s-p mixing of the Li orbitals, which is much stronger at the Li-NH geometry than for NH-Li [39].

Before examining the scattering dynamics, it is instructive to consider some analytical properties of the potential. For a Van der Waals potential that decays at long range as $-C_6/R^6$, a characteristic potential length may be defined [50],

$$R_{\rm vdW} = \frac{1}{2}\left(\frac{2\mu C_6}{\hbar^2}\right)^{1/4}. \tag{2}$$

Alternatively, the average scattering length $\bar{a}$, introduced by Gribakin and Flambaum [51], is

$$\bar{a} = \frac{4\pi}{\Gamma(1/4)^2} R_{\rm vdW} \approx 0.956 R_{\rm vdW}. \tag{3}$$

Gribakin and Flambaum showed that the scattering length follows

$$\frac{a}{\bar{a}} = 1 - \tan\left(\Phi - \frac{\pi}{8}\right), \tag{4}$$

where

$$\Phi = \int_{R_0}^{\infty} \left[-2\mu V(R)/\hbar^2\right]^{1/2} dR \tag{5}$$

is evaluated at threshold, with R_0 the inner classical turning point. When a is large and positive, the energy of the highest bound state is just below threshold and is given by

$$E_{\rm bind} = -\frac{\hbar^2}{2\mu(a-\bar{a})^2}. \tag{6}$$

If the potential is varied, by scaling or otherwise, the scattering length passes through a pole every time an s-wave bound state occurs at threshold. For Li(^2S)+NH($X^3\Sigma^-$), $C_6 = 164.9\, E_{\rm h} a_0^6$, and thus $R_{\rm vdW} = 10.89$ Å and $\bar{a}$ =10.42 Å, corresponding to an average elastic cross section of $\bar{\sigma}_{\rm elas} = 4\pi\bar{a}^2 = 1365$ Å^2.

3 Scattering Calculations

The Hamiltonian for a ^{2}S atom colliding with a rigid-rotor $^3\Sigma$ diatomic molecule may be written

$$\hat{H} = -\frac{\hbar^2}{2\mu}\frac{d^2}{dR^2} + \frac{\hat{L}^2}{2\mu R^2} + \hat{H}_{\rm mon} + \hat{H}_{\rm Z} + V_{\rm ss}(R) + V(R,\theta), \tag{7}$$

where $\hat{L}^2$ is the space-fixed end-over-end rotation operator for the atom and the diatomic molecule about one another, $\hat{H}_{\rm mon}$ is the field-free Hamiltonian for the diatomic monomer, $\hat{H}_{\rm Z}$ represents the Zeeman interaction, $V_{\rm ss}(R)$ is the anisotropic intermolecular spin-spin interaction, $V(R,\theta)$ is the intermolecular potential, and μ is the reduced mass of the colliding system. The approximation of treating NH as a rigid rotor is justified in more detail below.

The field-free monomer Hamiltonian for NH($X^3\Sigma^-$) is

$$\hat{H}_{\rm mon} = b_{\rm rot}\hat{n}^2 + \gamma_{\rm ns}\hat{n}\cdot s_{\hat{\rm NH}} + \lambda_{\rm ss}\left[\frac{4\pi}{5}\right]^{\frac{1}{2}}\sqrt{6}\sum_q (-1)^q Y_{2-q}(\boldsymbol{r})\left[s_{\rm NH}\otimes s_{\rm NH}\right]_q^{(2)} \tag{8}$$

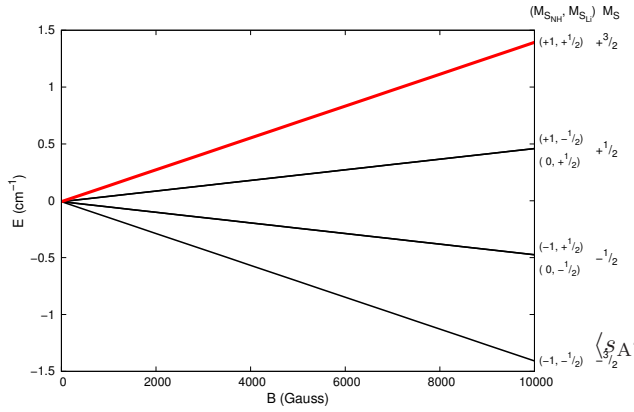

Fig. 2. (color online). Li(^2S)+NH($X^3\Sigma^-$) thresholds as a function of magnetic field. The spin-stretched ($m_{s_{\rm NH}} = +1, m_{s_{\rm Li}} = +\frac{1}{2}$) $M_S = +\frac{3}{2}$ state is shown in red.

where $\hat{n}$ and $\hat{s}_{\rm NH}$ are the NH rotation and electron spin angular momentum operators, $b_{\rm rot} = \hbar^2/2\mu r_{\rm mon}^2 = 16.343$ cm^{-1} is the NH rotational constant, $\gamma_{\rm ns} = -0.055$ cm^{-1} is the spin-rotation constant and $\lambda_{\rm ss} = 0.92$ cm^{-1} is the spin-spin interaction constant. The values of the spectroscopic constants for the vibrational ground state are from ref. [52]. The Zeeman Hamiltonian is

$$\hat{H}_{\rm Z} = g_e \mu_{\rm B} \hat{B} \cdot (\hat{s}_{\rm NH} + \hat{s}_{\rm Li}), \qquad (9)$$

where $\hat{B}$ is the magnetic field vector, $\mu_{\rm B}$ is the Bohr magneton and g_e is the electron g-factor. The anisotropic intermolecular spin-spin interaction can be expressed as

$$V_{\rm ss}(R) = \lambda(R)\left[\hat{s}_{\rm Li}\cdot\hat{s}_{\rm NH} - 3(\hat{s}_{\rm Li}\cdot\hat{e}_{\rm R})(\hat{s}_{\rm NH}\cdot\hat{e}_{\rm R})\right], \qquad (10)$$

where $\hat{s}_{\rm Li}$ and $\hat{s}_{\rm NH}$ are the spin angular momentum operators for the Li atom and the NH molecule respectively, $\hat{e}_{\rm R}$ is a unit vector along R, and $\lambda(R) = -E_{\rm h}\alpha^2/(R/a_0)^3$, where $\alpha \approx 1/137$ is the fine-structure constant.

We construct the collision Hamiltonian in the fully uncoupled basis set $|nm_n\rangle|s_{\rm NH}m_{s_{\rm NH}}\rangle|s_{\rm Li}m_{s_{\rm Li}}\rangle|LM_L\rangle$, where m_i is the projection of the angular momentum term s_i onto the space-fixed magnetic field axis. The matrix elements for NH monomer operators are the same as for scattering of NH from a closed-shell atom [53], with the addition of factors $\delta_{m_{s\rm A}m'_{s\rm A}}$. The intermolecular spin-spin interaction has matrix elements

$$\begin{aligned}\langle s_{\rm A}m_{s\rm A}s_{\rm B}m_{s\rm B}n_{\rm B}m_{n\rm B}LM_L|V_{\rm ss}|s_{\rm A}m'_{s\rm A}s_{\rm B}m'_{s\rm B}n'_{\rm B}m'_{n\rm B}L'M'_L\rangle \\ = \sqrt{30}\lambda(R)\delta_{n_{\rm B}n'_{\rm B}}\delta_{m_{n\rm B}m'_{n\rm B}}(-1)^{s_{\rm A}+s_{\rm B}-m_{s\rm A}-m_{s\rm B}-M_L} \\ [s_{\rm A}(s_{\rm A}+1)(2s_{\rm A}+1)s_{\rm B}(s_{\rm B}+1)(2s_{\rm B}+1)(2L+1)(2L'+1)]^{\frac{1}{2}} \\ \begin{pmatrix} L & 2 & L' \\ 0 & 0 & 0 \end{pmatrix} \sum_{q_1 q_2} \begin{pmatrix} L & 2 & L' \\ -M_L & -q_1-q_2 & M'_L \end{pmatrix} \\ \begin{pmatrix} 1 & 1 & 2 \\ q_1 & q_2 & -q_1-q_2 \end{pmatrix} \begin{pmatrix} s_{\rm A} & 1 & s_{\rm A} \\ -m_{s\rm A} & q_1 & m'_{s\rm A} \end{pmatrix} \begin{pmatrix} s_{\rm B} & 1 & s_{\rm B} \\ -m_{s\rm B} & q_2 & m'_{s\rm B} \end{pmatrix} \qquad (11)\end{aligned}$$

The total spin S of a system made up of an open-shell atom and an open-shell molecule can take values between $|s_{\rm A} - s_{\rm B}|$ and $s_{\rm A} + s_{\rm B}$. For Li–NH the allowed values are $S = \frac{1}{2}$ (doublet) and $\frac{3}{2}$ (quartet). The interaction potential $V_{\rm int}(R,\theta)$ may be written in terms of projection operators,

$$V_{\rm int}(R,\theta) = \sum_{S=-|s_{\rm A}+s_{\rm B}|}^{s_{\rm A}+s_{\rm B}} |S\rangle V_S(R,\theta)\langle S| \qquad (12)$$

and the matrix element of $V_{\rm int}(R,\theta)$ is

$$\begin{aligned}\langle s_{\rm A}m_{s\rm A}s_{\rm B}m_{s\rm B}n_{\rm B}m_{n\rm B}LM_L|V_{\rm int}(R,\theta)|s_{\rm A}m'_{s_{\rm A}}s_{\rm B}m'_{s\rm B}n'_{\rm B}m'_{n\rm B}L'M'_L\rangle \\ = \sum_S (-1)^{2s_{\rm A}+2s_{\rm B}-m_{s\rm A}-m_{s\rm B}-M_L}(2S+1) \\ \langle n_{\rm B}m_{n\rm B}LM_L|V_S(R,\theta)|n'_{\rm B}m'_{n\rm B}L'M'_L\rangle \\ \begin{pmatrix} s_{\rm A} & s_{\rm B} & S \\ m_{s\rm A} & m_{s\rm B} & -m_{s\rm A}-m_{s\rm B} \end{pmatrix} \begin{pmatrix} s_{\rm A} & s_{\rm B} & S \\ m'_{s\rm A} & m'_{s\rm B} & -m'_{s\rm A}-m'_{s\rm B} \end{pmatrix} \qquad (13)\end{aligned}$$

The doublet and quartet interaction potentials $V_S(R,\theta)$ have the same long-range coefficients, so become degenerate when the N atom and NH molecule are far enough apart that their valence shells do not overlap. In the present work we approximate the operator $V_{\rm int}(R,\theta)$ by taking $V_S = V_{3/2}$ for both spin states. This approximation is reasonable because we wish to focus on collisions between atoms and molecules in spin-stretched states, and $V_{1/2}$ has no matrix elements (diagonal or off-diagonal) involving such states. When this approximation is made, orthogonality relations for the $3j$ symbols reduce Eq. 13 to a form diagonal both in $m_{s\rm A}$ and $m_{s\rm B}$. The explicit expression for $\langle n_{\rm B}m_{n\rm B}LM_L|V_S(R,\theta)|n_{\rm B}m'_{n\rm B}L'M'_L\rangle$ is the same as for scattering of NH from a closed-shell atom [53], with the addition of factors $\delta_{m_{s\rm A}m'_{s\rm A}}$.

In a magnetic field, the lowest Li-NH threshold ($N = 0, s_{\rm NH} = 1, s_{\rm Li} = \frac{1}{2}$) splits into six Zeeman sub-levels, as shown in Figure 2. There is one $M_S = -\frac{3}{2}$ state, two degenerate $M_S = -\frac{1}{2}$ states, two degenerate $M_S = \frac{1}{2}$ states, and a single spin-stretched $M_S = \frac{3}{2}$ state.

In a magnetic field the projection of the total angular momentum $M_{\rm tot} = m_n + M_S + M_L$ is conserved. Thus in the rotational ground state $N = 0$, any change in M_S must be accompanied by a change in M_L. For s-wave scattering ($L = 0$) from the spin-stretched $M_S = +\frac{3}{2}$ state, this requires that $L = 0 \to L \geq 2$. Thus the dominant outgoing channels are $|M_S = \pm\frac{1}{2}, L = 2\rangle$ and $|M_S = -\frac{3}{2}, L = 4\rangle$, which have centrifugal barriers that suppress inelastic scattering at low energies and magnetic fields. The heights of the centrifugal barriers are approximately $E_{\rm cf}^L = (\hbar^2 L(L+1)/\mu)^{\frac{3}{2}}(54C_6)^{-\frac{1}{2}}$, which for LiNH are $E_{\rm cf}^2 = 60$ mK and $E_{\rm cf}^4 = 368$ mK.

For magnetically trapped spin-stretched states, collisional spin relaxation to other Zeeman states will result in heating and/or loss of molecules from the trap. Spin relaxation occurs via two mechanisms. The first is via the direct coupling of the incident state to outgoing states through the anisotropic spin-spin interaction, by a similar mechanism to spin relaxation in collisions between alkali-metal atoms. The second occurs via the interplay of the

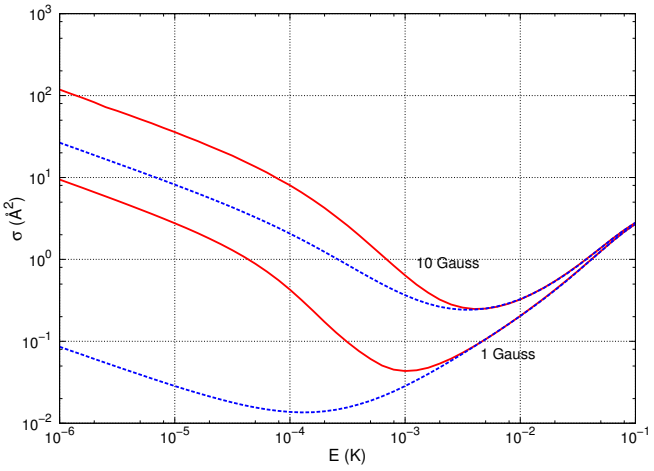

Fig. 3. (color online). S-wave total inelastic cross sections calculated as a function of collision energy for $R_{\rm AX} > R_{\rm max} = 50$ Å (blue, dashed) and $R_{\rm AX} < R_{\rm max} = 600$ Å (red, solid) for magnetic fields of 1 and 10 Gauss. $R_{\rm AX}(1\ {\rm G}) = 476$ Å and $R_{\rm AX}(10\ {\rm G}) = 150$ Å.

potential anisotropy and the intramolecular NH spin-spin interaction [54], which results in an inelastic cross section proportional to $1/b_{\rm rot}^2$ [55,56].

We have carried out low-energy quantum scattering calculations using the MOLSCAT package [57], as modified to handle collisions in magnetic fields [53]. Sets of coupled-channel equations are constructed for each $M_{\rm tot}$ in the uncoupled basis set described above. Solutions to the coupled-channel equations are then propagated over a grid in R, using the hybrid log-derivative method of Alexander and Manolopoulos [58], which in the short-range region ($R_{\rm min} \le R < R_{\rm mid}$) uses a fixed-step-size log-derivative propagator and in the long-range region ($R_{\rm mid} \le R \le R_{\rm max}$) a variable step-size Airy propagator. At $R_{\rm max}$, the log-derivative solutions are transformed into the basis set of asymptotic eigenfunctions and matched to scattering boundary conditions to obtain the S-matrix $S^{\rm M_{tot}}$. The scattering cross sections between levels i and f are then obtained from

$$\sigma_{i\to f} = \frac{\pi}{k_i^2} \sum_{M_{\rm tot} L_i L_f} \left| \delta_{if}\delta_{L_i L_f} - S^{M_{\rm tot}}_{iL_i fL_f} \right|^2, \qquad (14)$$

where k_i is the wave vector in the incident channel, $k_i^2 = 2\mu(E - E_i)/\hbar^2$.

The anisotropic intermolecular spin-spin interaction directly couples the incident s-wave channel $M_S = +\frac{3}{2}, L = 0$ to the two $M_S = +\frac{1}{2}, L = 2$ channels and to the $(-1, +\frac{1}{2}), M_S = -\frac{1}{2}, L = 2$ channel. Since the $L = 2$ channels have barriers at long range, there are narrowly avoided crossings between the channel adiabats [59] at very long range when the kinetic energy release is small (at low magnetic field). If the long-range behaviour in both the $L = 0$ and $L = 2$ channels is of the form

$$V(R) \xrightarrow[R\to\infty]{} \frac{\hbar^2 L(L+1)}{2\mu R^2} - \frac{C_6}{R^6} + \mathcal{O}(R^{-7}), \qquad (15)$$

these avoided crossings are at a distance $R_{\rm AX}$ such that

$$g_e \mu_{\rm B} B \Delta M_S = \frac{\hbar^2 \left[L_f(L_f+1) - L_i(L_i+1)\right]}{2\mu R_{\rm AX}^2}, \qquad (16)$$

where $g_e\mu_{\rm B}B\Delta M_S$ is the energy separation of the two adiabats due to the magnetic field B, L_i and L_f are the values of L in the incoming and outgoing channels, and $\Delta M_S = M_{S_f} - M_{S_i}$. To account correctly for the intermolecular spin-spin coupling, the scattering solutions need to be propagated out beyond the largest value of $R_{\rm AX}$. Figure 3 shows the effect of placing $R_{\rm max} < R_{\rm AX}$ and $R_{\rm AX} < R_{\rm max}$ on the total inelastic s-wave cross sections as a function of collision energy. We consider only magnetic fields relevant to sympathetic cooling down to 1 G, at which point the largest $R_{\rm AX} = 476$ Å, and thus the propagation parameters $R_{\rm min} = 1.8$ Å, $R_{\rm mid} = 12.5$ Å and $R_{\rm max} = 600$ Å were used throughout.

Low-energy scattering depends strongly on the details of the potential energy surface. Thus when converging the basis set for the scattering calculations we need consider the uncertainty in the interaction potential as well as convergence with respect to the variables $n_{\rm max}$ and $L_{\rm max}$ that govern the basis set size [60]. To explore the convergence with respect to the potential we introduce a scaling factor $\lambda_{\rm scl}$ that allows the interaction potential to be varied within its error bounds,

$$V^{\rm scaled}(R,\theta) = \lambda_{\rm scl} V(R,\theta). \qquad (17)$$

Since the main features of the cross sections are determined by the scattering length and the positions of bound states that cause resonances, both of which are tuned by $\lambda_{\rm scl}$, scaling the potential in this way is sufficient to explore the range of possible collision behaviour. This also justifies fixing the NH bond length r in our calculations: the collisions are approximately vibrationally adiabatic, and allowing r to relax would simply deepen the potential slightly and correspond approximately to a value of $\lambda_{\rm scl} > 1$.

Figure 4 shows the potential-dependence of the s-wave spin-stretched elastic scattering cross section for the three basis sets $n_{\rm max} = 6, L_{\rm max} = 6$ (645 channels), $n_{\rm max} = 6, L_{\rm max} = 8$ (937 channels), and $n_{\rm max} = 8, L_{\rm max} = 8$ (1403 channels) at a collision energy of 10^{-6} K and a magnetic field of 10 G. Calculations with $n_{\rm max} = 8, L_{\rm max} = 10$ (1887 channels) gave results essentially identical to those with $n_{\rm max} = 8, L_{\rm max} = 8$. The computer time scales as the number of channels cubed. It may be seen that, for all three basis sets, the elastic cross sections fluctuate about the average cross section $\bar{\sigma}_{\rm elas}$ and the total inelastic cross sections have peaks at corresponding positions. The fluctuations (resonances) have quite similar form for different basis sets, but the positions of the resonances are shifted. This is similar to the result obtained by Janssen *et al.* [60] for NH-NH.

It is clear that basis sets smaller than $n_{\rm max} = 8, L_{\rm max} = 8$ do not give "converged" results for a specific interaction potential. However, the calculated interaction potential is itself probably accurate only to about ±5%. Even a fully

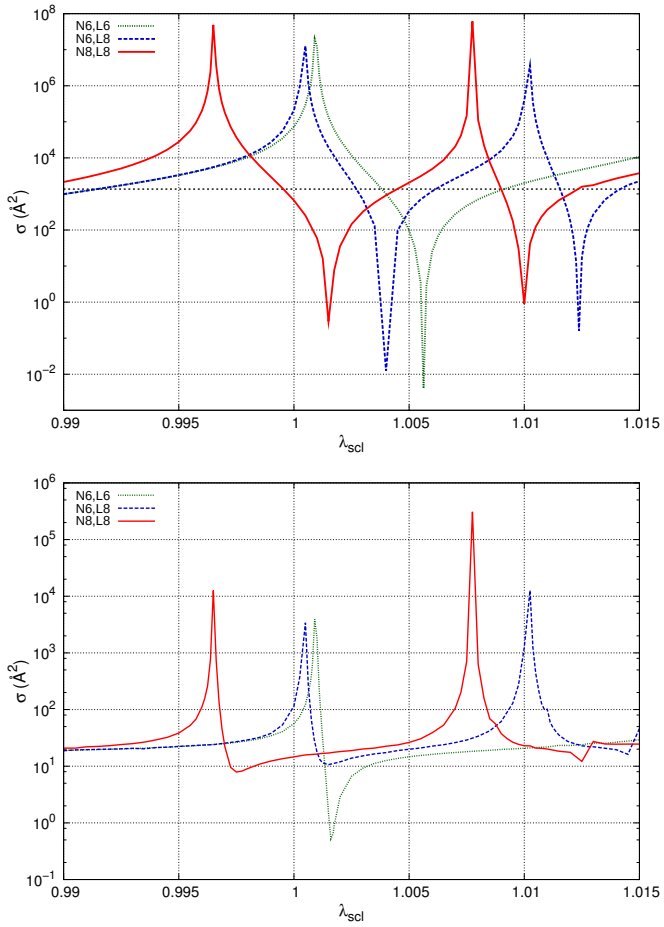

Fig. 4. (color online). Spin-stretched s-wave elastic (upper panel) and inelastic (lower panel) cross sections calculated for basis sets with $n_{\max} = 6, L_{\max} = 6$ (green, dotted), $n_{\max} = 6, L_{\max} = 8$ (blue, dashed), and $n_{\max} = 8, L_{\max} = 8$ (red, solid), as a function of the potential scaling factor $\lambda_{\rm scl}$ at a collision energy of 10^{-6} K and a magnetic field strength of 10 Gauss. The average cross section $\bar{\sigma}_{\rm elas} = 4\pi\bar{a}^2 = 1365$ Å^2 is also shown (black, heavy-dots).

converged basis set would therefore not give reliable predictions of numerical values for elastic (or inelastic) cross sections in the ultracold regime. Nevertheless, *even an unconverged basis set* reliably predicts the *probability* that the elastic and inelastic cross sections will lie in a particular range of values, and thus the likelihood that sympathetic cooling can succeed. Until the actual cross sections are measured, we have to accept this uncertainty in the results, and until then there is no point in using very expensive basis sets that aim for complete convergence.

The converged $n_{\max} = 8, L_{\max} = 8$ basis is computationally too expensive for calculations involving p-wave and higher partial-wave contributions, which are required at temperatures above 10 μK. The smaller and more computationally manageable $n_{\max} = 6, L_{\max} = 8$ has therefore been used in the remainder of this work. Figure 5 shows the dependence of the elastic and total inelastic

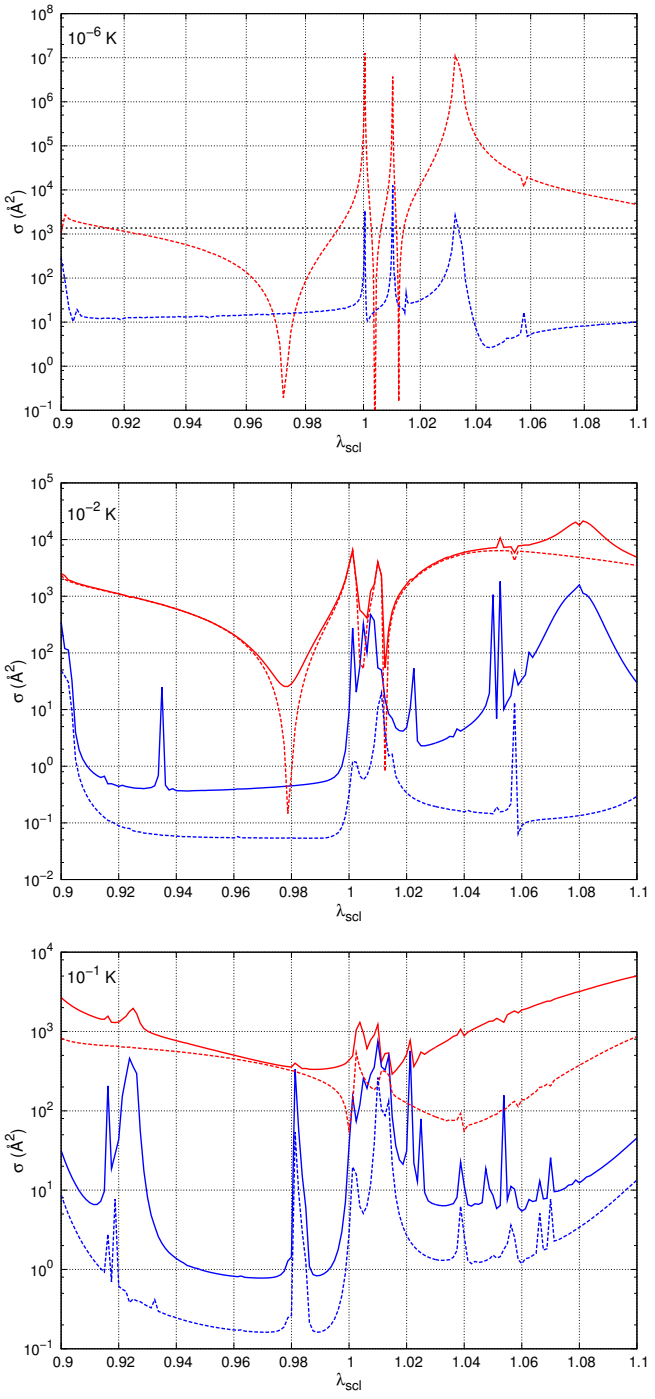

Fig. 5. (color online). Dependence of the elastic (red) and total inelastic (blue) cross sections on the potential scaling factor $\lambda_{\rm scl}$ at collision energies of 1 μK (top), 10 mK (center) and 100 mK (bottom) at a magnetic field strength of 10 G. The s-wave contribution to each cross section is shown as a dashed line (and is the only significant contribution at 10^{-6} K). The average s-wave cross section $\bar{\sigma}_{\rm elas} = 4\pi\bar{a}^2 = 1365$ Å^2 is shown as a dotted black line. The calculations use the basis set with $n_{\max} = 6, L_{\max} = 8$.

cross sections with this basis set for a wider range of $\lambda_{\rm scl}$ for collision energies of 1 μK, 10 mK and 100 mK: it may be seen that the higher partial waves that contribute at higher energies "fill in" the deep dips that occur in the s-wave cross sections, but that additional structure appears at higher energy because of resonances in higher partial waves.

4 Prospects for Sympathetic Cooling

In a simple hard-sphere model of sympathetic cooling, neglecting inelastic collisions, the temperature relaxes towards equilibrium and reaches a $1/e$ point after $(m_1 + m_2)^2/2m_1m_2$ collisions [25], where m_1 and m_2 are the masses of the two species. For sympathetic cooling to be successful we need the ratio of elastic to inelastic cross sections to be much larger than this. The general rule of thumb is that the ratio of the elastic to the total inelastic cross sections, $\gamma = \sigma_{\rm elas}/\sigma_{\rm inelas}$, must be greater than about 100.

Figure 6 shows the spin-stretched elastic and total inelastic cross sections, incorporating all s, p, and d partial wave contributions ($L = 0, 1, 2$) for the original *ab initio* potentials with $\lambda_{\rm scl} = 1$ and for representative scaled potentials with $\lambda_{\rm scl} = 0.96$ and 0.915, chosen to give $a = 0.3\overline{a}$ and $a = \overline{a}$, respectively. The potential with $\lambda_{\rm scl} = 1$ has $a = -12.5\bar{a}$, and thus an atypically large value of the elastic cross section. The spd basis set gives convergence of the partial-wave sum in cross sections for collision energies up to about 60 mK. At low magnetic fields the kinetic energy release (i.e. the Zeeman splitting between the incoming and outgoings channels) is less than the height of the barriers in the outgoing channels, so that the inelastic cross section is suppressed. As the magnetic field is decreased, the Zeeman splitting decreases, the centrifugal suppression increases, and the inelastic cross section decreases. The dominant elastic processes are $\Delta L = 0$, so the elastic cross section does not display significant field-dependence. It may also be seen from Figure 6 that the ratio γ is in excess of 100 for low magnetic fields and a wide range of collision energies up to about 30 mK. However, due to the presence of the intermolecular spin-spin interaction [59], the reduction of the inelastic cross section at low fields is not as dramatic as in Mg+NH [40].

To assess the prospect of sympathetic cooling over the range of possible potentials, Figure 7 shows contour plots of γ as a function of the collision energy and magnetic field strength for a variety of λ values, chosen to give a range of scattering lengths from $-12.5\bar{a}$ to $+12.5\bar{a}$. It may be seen that the majority of possible potentials give favourable values of γ over a wide range of fields and energies. The unfavourable potential at the upper right is also atypical: it has $a = 0.1\bar{a}$, so that the s-wave elastic scattering cross section is a factor of 100 below the typical value of $4\pi\bar{a}^2$. Such unfavourable behaviour might occur for any system, but is not very likely.

In an unbiased magnetic quadrupole trap, with a field zero at the center, the molecules in the $m_{s_{\rm NH}} = 1$ state at

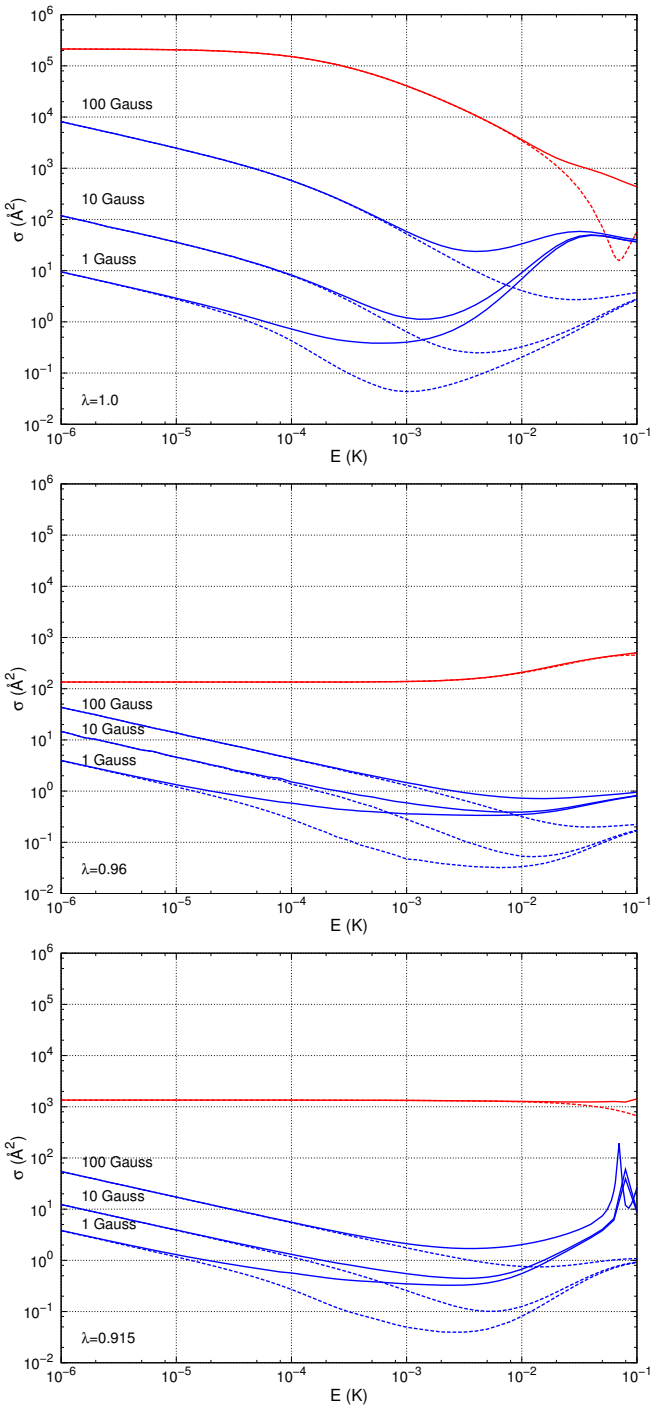

Fig. 6. (color online). Li+NH spin-stretched elastic (solid, red) and total inelastic (solid, blue) cross sections as a function of collision energy for various magnetic fields, for the potentials with $\lambda_{\rm scl} = 1$, 0.96 and 0.915, corresponding to $a = -12.5\overline{a}$, $0.3\overline{a}$, $\overline{a}$, respectively. The cross sections include all s, p, and d-wave ($L = 0, 1, 2$) contributions. The s-wave elastic (dashed,red) and total inelastic (dashed, blue) cross sections are also shown.

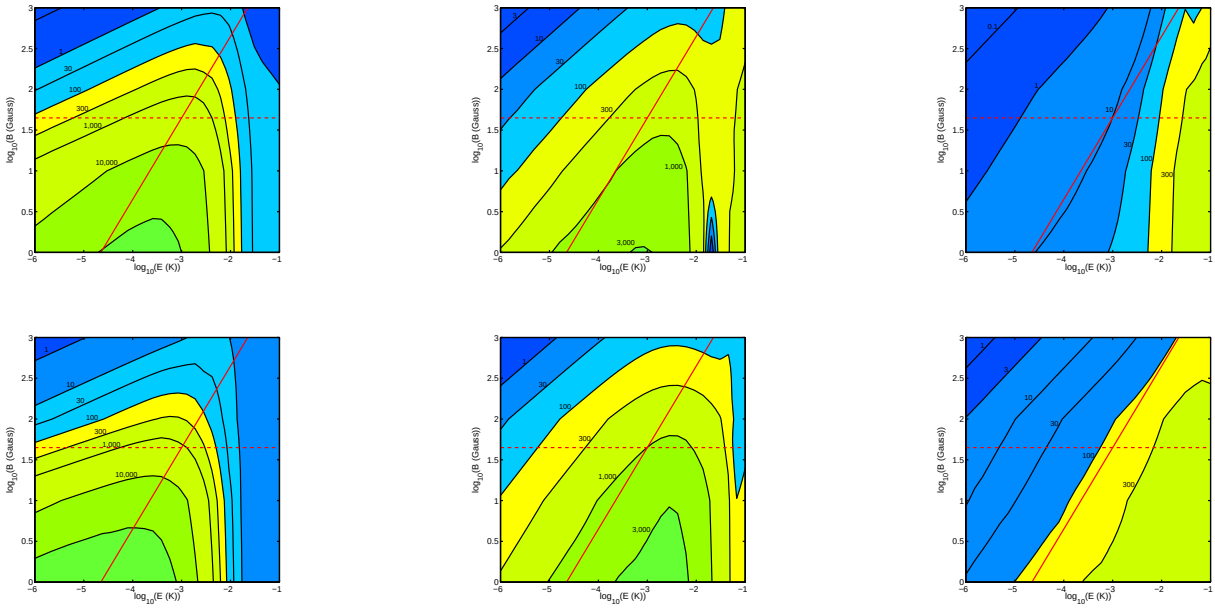

Fig. 7. (color online). Contour plots of the ratio γ of the elastic to total inelastic cross sections including all s, p and d-wave contributions. Contour plots are shown for six different values of the potential scaling factor (clockwise from the top left): (a) $\lambda_{\rm scl} = 1$, $a = -12.5\bar{a}$. (b) $\lambda_{\rm scl} = 0.9915$, $a = -\bar{a}$, (c) $\lambda_{\rm scl} = 0.97$, $a = 0.1\bar{a}$, (d) $\lambda_{\rm scl} = 0.96$, $a = 0.3\bar{a}$, (e) $\lambda_{\rm scl} = 0.915$, $a = \bar{a}$, and (f) $\lambda_{\rm scl} = 1.00078$, $a = 12.5\bar{a}$, The solid red lines show the maximum field sampled by the spin-stretched state of the molecules, $B = 6k_{\rm B}T_{\rm NH}/g_e\mu_{\rm B}$ and the dashed red line shows a similar boundary for Li atoms at $T_{\rm Li} = 1$ mK.

a temperature $T_{\rm NH}$ will have a Boltzmann density distribution

$$\frac{\rho}{\rho_0} = \exp\left(-\frac{g_e\mu_{\rm B}Bm_{s_{\rm NH}}}{k_{\rm B}T_{\rm NH}}\right). \qquad (18)$$

At a given temperature on the energy axis of the contour plots in Figure 7 less than 1% of molecules will experience a magnetic field greater than $B = 6k_{\rm B}T_{\rm NH}/g_e\mu_{\rm B}$, which is shown as a solid red line. If the atomic cloud occupied the same volume as the molecular cloud, the large majority of collisions would occur at energy/field combinations below this line. However, at the start of sympathetic cooling the Li is likely to be substantially colder than the NH, probably 1 mK or less. The Doppler limit for Li is 140 μK. The magnetic moment of ^{7}Li in its $F = 2$, $M_F = 2$ state is only half that of NH, but nevertheless it is likely that the Li cloud will be significantly smaller. Li-NH collisions will take place only where both species are present, near the centre of the trap where fields are low. This will reduce the frequency of collisions but may nevertheless be advantageous because it will mean that collisions mostly take place in regions well below the solid red line. Over 99% of Li atoms at a temperature $T_{\rm Li}$ will occupy regions of the trap with fields less than $B = 12k_{\rm B}T_{\rm Li}/g_e\mu_{\rm B}$, and this boundary is shown in Figure 7 as a dashed red line for Li at 1 mK. For many potentials the inelasticity in this region remains low to temperatures above 100 mK at fields below 100 G.

It can be seen from Figure 7 that the contour plots depend mostly on the magnitude of the scattering length and not on its sign, because the s-wave elastic cross section is proportional to the square of the scattering length. There are small deviations from this: for $a \approx \bar{a}$ there is a p-wave resonance around 50 mK, and for $a \approx -\bar{a}$ there is a d-wave resonance around 50 mK and 500 G. If the real potential is such that a is accidentally close to zero, such as for $\lambda_{\rm scl} = 0.97$, sympathetic cooling will not succeed because of the small elastic cross section. However as $|a|/\bar{a}$ increases to "typical" values close to 1 (such as for $\lambda_{\rm scl} = 0.96$), sympathetic cooling has a good chance of success. For all potentials with $|a|/\bar{a} \geq 1$ it can be seen that, once sympathetic cooling has started and the sample of molecules is cooled to sub-millikelvin temperatures, γ increases and the molecules become increasingly stable to spin-relaxation. The temperature at which sympathetic cooling begins to be effective depends quite strongly on the potential, but for some potentials it is as high as 100 mK.

Changing the reduced mass of the collision system has an effect quite similar to scaling the potential [61]. Thus if the scattering length for one isotopic combination proves to be too small to allow sympathetic cooling to succeed, another combination may well be more successful.

A further important consideration in a sympathetic cooling experiment concerns the absolute collision rate. As seen above, the elastic cross section in the ultracold regime fluctuates dramatically near Feshbach resonances but its "background" value is $4\pi\bar{a}^2$, which for Li+NH is 1365 Å^2. The elastic cross section drops off at higher energy for some potentials, but in most cases it does not change by more than a factor of 3 from $4\pi\bar{a}^2$ (in either direction) at collision energies around 100 mK. At this temperature,

with a reasonable Li atom density of 10^{10} cm^{-3} and an elastic cross section of 10^3 Å, each molecule will experience a collision with a Li atom once every 0.8 ms. However, this time will be extended if only part of the molecular cloud overlaps with the atomic trap. In a magnetic quadrupole trap with a molecular temperature much higher than the atomic temperature, the overlap between the two clouds will be quite poor. This might be alleviated by using a trap of Ioffe-Pritchard type, with a finite magnetic field at the bottom of the trap. This would have the beneficial side-effect of preventing Majorana losses [62,63] at the center of the trap. As cooling progresses, the molecular cloud will collapse towards the center of the trap, so the overlap with the atomic trap will improve. As this occurs, the bias field of the Ioffe-Pritchard trap can be reduced to increase the density and the corresponding collision rate.

5 Conclusions

We have calculated the quartet potential energy surface for NH interacting with Li and used it to calculate elastic and inelastic cross sections for collisions between cold NH and Li in magnetically trappable spin-stretched states. The potential energy surface is highly anisotropic, with a well depth about 1800 cm^{-1} at the Li-NH geometry but only 113 cm^{-1} and the NH-Li geometry. The strong anisotropy drives spin-relaxation collisions that are considerably faster than in systems such as Mg-NH and He-NH, but are nevertheless suppressed by centrifugal barriers when both species are in spin-stretched states.

We have explored the dependence of the collision properties on the potential energy surface, or equivalently on the reduced mass of the colliding system. In the ultracold regime, both the elastic and inelastic (spin-relaxation) cross sections show dramatic fluctuations as the potential is varied, due to Feshbach resonances that occur as a bound state passes through zero energy. The potential-dependence is considerably reduced at higher energies, when higher partial waves contribute to the scattering. The major effect of using an unconverged basis set in the scattering calculations is to shift the positions of the resonances without changing their general behaviour.

We have calculated the ratio of elastic and inelastic (spin-relaxation) cross sections, as a function of collision energy and magnetic field, for a variety of potential energy surfaces. This ratio is key to the success of sympathetic cooling, because spin-relaxation cross sections convert internal energy into relative translation of the colliding species and thus cause trap loss. We find that most (but not all) potential energy surfaces produce ratios that are favorable for sympathetic cooling, provided the molecules can be precooled to a temperature around 20 mK. The exceptions are potentials where the scattering length is accidentally near zero, which produce small elastic cross sections in the ultracold regime. If this unlucky situation occurs in practice, it can probably be avoided by using a different isotopic combination of NH and/or Li.

It is important to consider the overlap between the atomic and molecular traps. If both species are held in a magnetic quadrupole trap and the atoms are initially much colder than the molecules, the atomic cloud will be much smaller than the molecular cloud. This may be advantageous because it means that atom-molecule collisions will take place only at the low magnetic fields sampled by the atoms, and for many potentials such low-field collisions have low inelasticity even at temperatures around 10 mK. However, there is a price to pay because poor overlap extends the time needed for sympathetic cooling. This might be alleviated by using a Ioffe-Pritchard trap to increase the size of the atomic cloud in the early stages of cooling.

Acknowledgments

We are grateful to Liesbeth Janssen for valuable discussions. This work is supported by EPSRC under the collaborative project CoPoMol of the ESF EUROCORES Programme EuroQUAM.

References

1. M.H. Anderson, J.R. Ensher, M.R. Matthews, C.E. Wieman, E.A. Cornell, Science **269**(5221), 198 (1995)
2. K.B. Davis, M.O. Mewes, M.R. Andrews, N.J. VanDruten, D.S. Durfee, D.M. Kurn, W. Ketterle, Phys. Rev. Lett. **75**(22), 3969 (1995)
3. J. Doyle, B. Friedrich, R.V. Krems, F. Masnou-Seeuws, Eur. Phys. J. D **31**(2), 149 (2004)
4. R.V. Krems, Int. Rev. Phys. Chem. **24**(1), 99 (2005)
5. B. Friedrich, J.M. Doyle, Chem. Phys. Chem. **10**(4), 604 (2009)
6. J.J. Hudson, B.E. Sauer, M.R. Tarbutt, E.A. Hinds, Phys. Rev. Lett. **89**(2), 023003 (2002)
7. H. Bethlem, W. Ubachs, Faraday Discussions **142**, 25 (2009)
8. D. DeMille, Phys. Rev. Lett. **88**(6), 067901 (2002)
9. M.T. Bell, T.P. Softley, Mol. Phys. **107**(2), 99 (2009)
10. W.D. Phillips, Rev. Mod. Phys. **70**(3), 721 (1998)
11. H.L. Bethlem, G. Meijer, Int. Rev. Phys. Chem. **22**(1), 73 (2003)
12. J.M. Hutson, P. Soldán, Int. Rev. Phys. Chem. **25**(4), 497 (2006)
13. J.G. Danzl, E. Haller, M. Gustavsson, M.J. Mark, R. Hart, N. Bouloufa, O. Dulieu, H. Ritsch, H.C. Nägerl, Science **321**, 1062 (2008)
14. F. Lang, K. Winkler, C. Strauss, R. Grimm, J. Hecker Denschlag, Phys. Rev. Lett. **101**, 133005 (2008)
15. K.K. Ni, S. Ospelkaus, M.H.G. de Miranda, A. Pe'er, B. Neyenhuis, J.J. Zirbel, S. Kotochigova, P.S. Julienne, D.S. Jin, J. Ye, Science **322**, 231 (2008)
16. J.G. Danzl, M.J. Mark, E. Haller, M. Gustavsson, R. Hart, J. Aldegunde, J.M. Hutson, H.C. Nägerl, Nature Phys. (2010)
17. J.D. Weinstein, R. deCarvalho, T. Guillet, B. Friedrich, J.M. Doyle, Nature **395**(6698), 148 (1998)
18. D. Egorov, W.C. Campbell, B. Friedrich, S.E. Maxwell, E. Tsikata, L.D. van Buuren, J.M. Doyle, Eur. Phys. J. D **31**(2), 307 (2004)

19. W.C. Campbell, E. Tsikata, H.I. Lu, L.D. van Buuren, J.M. Doyle, Phys. Rev. Lett. **98**(21), 213001 (2007)
20. E. Tsikata, W.C. Campbell, M.T. Hummon, H.I. Lu, J.M. Doyle, New J. Phys. **12**(6), 065028 (2010)
21. M.T. Hummon, W.C. Campbell, H.I. Lu, E. Tsikata, Y. Wang, J.M. Doyle, Phys. Rev. A **78**(5), 050702 (2008)
22. S. Hoekstra, M. Metsala, P.C. Zieger, L. Scharfenberg, J.J. Gilijamse, G. Meijer, S.Y.T. van de Meerakker, Phys. Rev. A **76**(6), 063408 (2007)
23. S.Y.T. van de Meerakker, R.T. Jongma, H.L. Bethlem, G. Meijer, Phys. Rev. A **64**(4), 041401(R) (2001)
24. D.J. Haxton, S.A. Wrathmall, H.J. Lewandowski, C.H. Greene, Phys. Rev. A **80**, 022708 (2009)
25. R. deCarvalho, J. Kim, J.D. Weinstein, J.M. Doyle, B. Friedrich, T. Guillet, D. Patterson, Eur. Phys. J. D **7**, 289 (1999)
26. D.J. Larson, J.C. Bergquist, J.J. Bollinger, W.M. Itano, D.J. Wineland, Phys. Rev. Lett. **57**(1), 70 (1986)
27. A. Ostendorf, C.B. Zhang, M.A. Wilson, D. Offenberg, B. Roth, S. Schiller, Phys. Rev. Lett. **97**(24), 243005 (2006)
28. C.J. Myatt, E.A. Burt, R.W. Ghrist, E.A. Cornell, C.E. Wieman, Phys. Rev. Lett. **78**(4), 586 (1997)
29. A.G. Truscott, K.E. Strecker, W.I. McAlexander, G.B. Partridge, R.G. Hulet, Science **291**(5513), 2570 (2001)
30. G. Modugno, G. Ferrari, G. Roati, R.J. Brecha, A. Simoni, M. Inguscio, Science **294**(5545), 1320 (2001)
31. P. Soldán, J.M. Hutson, Phys. Rev. Lett. **92**(16), 163202 (2004)
32. M. Lara, J.L. Bohn, D. Potter, P. Soldán, J.M. Hutson, Phys. Rev. Lett. **97**, 183201 (2006)
33. M. Lara, J.L. Bohn, D.E. Potter, P. Soldán, J.M. Hutson, Phys. Rev. A **75**, 012704 (2007)
34. M. Tacconi, E. Bodo, F.A. Gianturco, Theor. Chem. Acc. **117**, 649 (2007)
35. M. Tacconi, E. Bodo, F.A. Gianturco, Phys. Rev. A **75**, 012708 (2007)
36. M. Tacconi, L. Gonzalez-Sanchez, E. Bodo, F.A. Gianturco, Phys. Rev. A **76**, 032702 (2007)
37. P.S. Żuchowski, J.M. Hutson, Phys. Rev. A **78**, 022701 (2008)
38. P.S. Żuchowski, J.M. Hutson, Phys. Rev. A **79**, 062708 (2009)
39. P. Soldán, P.S. Żuchowski, J.M. Hutson, Faraday Discuss. **142**, 191 (2009)
40. A.O.G. Wallis, J.M. Hutson, Phys. Rev. Lett. **103**, 183201 (2009)
41. T.E. Mehlstäubler, K. Moldenhauer, M. Riedmann, N. Rehbein, J. Friebe, E.M. Rasel, W. Ertmer, Phys. Rev. A **77**(2), 021402(R) (2008)
42. P.J. Knowles, C. Hampel, H.J. Werner, J. Chem. Phys. **99**(7), 5219 (1993)
43. J. Čížek, J. Chem. Phys. **45**(11), 4256 (1966)
44. T.H. Dunning, Jr., J. Chem. Phys. **90**, 1007 (1989)
45. H.J. Werner, P.J. Knowles, R. Lindh, M. Schütz, P. Celani, T. Korona, F.R. Manby, G. Rauhut, R.D. Amos, A. Bernhardsson et al., MOLPRO*, version 2006.1: A package of ab initio programs* (2006), see http://www.molpro.net
46. S.F. Boys, F. Bernardi, Mol. Phys. **19**(4), 553 (1970)
47. C.R. Brazier, R.S. Ram, P.F. Bernath, J. Mol. Spectrosc. **120**(2), 381 (1986)
48. T.S. Ho, H. Rabitz, J. Chem. Phys. **104**(7), 2584 (1996)
49. P. Soldán, J.M. Hutson, J. Chem. Phys. **112**(9), 4415 (2000)
50. K.M. Jones, E. Tiesinga, P.D. Lett, P.S. Julienne, Rev. Mod. Phys. **78**, 483 (2006)
51. G.F. Gribakin, V.V. Flambaum, Phys. Rev. A **48**, 546 (1993)
52. M. Mizushima, *Theory of Rotating Diatomic Molecules* (Wiley, New York, 1975)
53. M.L. González-Martínez, J.M. Hutson, Phys. Rev. A **75**, 022702 (2007)
54. R.V. Krems, A. Dalgarno, J. Chem. Phys. **120**(5), 2296 (2004)
55. H. Cybulski, R.V. Krems, H.R. Sadeghpour, A. Dalgarno, J. Kłos, G.C. Groenenboom, A. van der Avoird, D. Zgid, G. Chałasiński, J. Chem. Phys. **122**(9), 094307 (2005)
56. W.C. Campbell, T.V. Tscherbul, H.I. Lu, E. Tsikata, R.V. Krems, J.M. Doyle, Phys. Rev. Lett. **102**(1), 013003 (2009)
57. J.M. Hutson, S. Green, *MOLSCAT computer program, version 14*, distributed by Collaborative Computational Project No. 6 of the UK Engineering and Physical Sciences Research Council (1994)
58. M.H. Alexander, D.E. Manolopoulos, J. Chem. Phys. **86**, 2044 (1987)
59. L.M.C. Janssen, P.S. Żuchowski, A. van der Avoird, G.C. Groenenboom, J.M. Hutson, arXiv:1012.2814 (2010)
60. L.M.C. Janssen, P.S. Żuchowski, A. van der Avoird, J.M. Hutson, G.C. Groenenboom, arXiv:1012.0804 (2010)
61. P.S. Żuchowski, J.M. Hutson, Phys. Chem. Chem. Phys. **13**, 3669 (2011)
62. E. Majorana, Nuovo Cimento **9**, 43 (1932)
63. W. Petrich, M.H. Anderson, J.R. Ensher, E.A. Cornell, Phys. Rev. Lett. **74**, 3352 (1995)